# Thermal and Surface Characterization of Polyurethane–Urea Clay Nanocomposite Coatings

**B. Sreedhar,[1] D. K. Chattopadhyay,[2] V. Swapna[1]**

[1]*Inorganic and Physical Chemistry Division, Indian Institute of Chemical Technology, Hyderabad 500007, India*
[2]*Organic Coatings and Polymers Division, Indian Institute of Chemical Technology, Hyderabad 500007, India*

Received 24 May 2005; revised 18 July 2005; accepted 1 September 2005
DOI 10.1002/app.23140
Published online in Wiley InterScience (www.interscience.wiley.com).

**ABSTRACT:** This paper reports synthesis and characterization of polyurethane–urea (PU-urea) and the nanocomposites derived from the PU-urea with silicate clays. Organophilic montmorillonite cotreated by cetyl trimethyl ammonium bromide (CTAB) was synthesized and used to prepare PU-urea/montmorillonite nanocomposites coatings. PU-ureas were prepared from polyethylene glycol (PEG), polypropylene glycol (PPG), trimethylol propane (TMP), and 4,4′-diphenylmethane diisocyanate (MDI) by reacting excess diisocyanate with polyether glycols. The excess isocyanate of the prepolymers was cured with atmospheric moisture. The synthesized moisture cured PU-urea and nanocomposites were characterized by Fourier transform infrared (FTIR) spectroscopy, thermogravimetric analysis (TGA), differential scanning calorimetric (DSC), and angle resolved X-ray photoelectron spectroscopy (AR-XPS). The thermal stability of the PU-urea nanocomposites was higher relative to the mother PU-urea films. DSC results showed a slight enhancement in the soft segment glass transition temperature after 3 wt % clay loading. The surface properties showed an enrichment of the soft segment toward the surface. An enhancement in the hard segment composition in the nanocomposite coatings has resulted in enhancing the phase mixing process.  J Appl Polym Sci 100: 2393–2401, 2006

**Key words:** polyurethane; clay; nanocomposites; TGA; XPS

## INTRODUCTION

Segmented polyurethane ureas (PU-urea) are block copolymers with alternating soft and hard blocks, which due to structural differences separate into two phases. The soft segments are derived from a macrodiol and the hard ones are obtained from the reaction of a diisocyanate with atmospheric moisture or diamine chain extender. The length of the soft segment results from the molecular weight of the macrodiols, whereas the hard segment length depends on the kind and molar ratio of the compounds used in the reaction. Hard segment plays the role of physical crosslinks and act as higher modulus filler in the low modulus soft matrix, whereas the soft phase gives extensibility to the polymer. A wide variety of fillers, whiskers, and fibers as well as clay and wollastonites are being applied in polyurethane formulations to reduce cost and to reinforce the polyurethane matrix that results in improved hardness, strength, and stiffness.[1] The improved mechanical, thermal, and permeability properties are mainly due to the conversion of a large fraction of the polymer matrix near their surfaces into an interphase of different properties resulting in a change in its morphology.[2] In general, the properties of filled polyurethanes are dependent upon filler shape, size, and the extent of interfacial coupling. To meet the modern technological demands in this arena, the size of the fillers should be reduced to the nanometer scale. As the size reduces into the nanometer range, the composite materials exhibit peculiar and interesting mechanical and physical properties, for example, increased mechanical strength, superior hardness, enhanced thermal stability, higher specific heat, and electrical resistivity compared with conventional coarse grained counterparts.[3] These improved and unexpected hybrid property results from the synergistically derived interface by the two components and has shown increasing attention in the scientific community during the last decade. A few studies on polyurethane nanocomposites, in which the synthesis and mechanical properties were described, have been reported.[4–16] Elastomeric PU/clay nanocomposite was first reported by Wang and Pinnavaia.[5] They focused on the compatibility between organo-clay and polyols. They found that the montmorillonite clay exchanged with long chain onium ions (carbon number $\geq 12$) had a good compatibility with several polyols commonly used for synthesizing polyurethane, and therefore a maximum benefit from nanolayer dispersal and reinforcement was observed.[5] In an earlier observation, Pinnavaia[15] suggested that increasing the alkyl chain

*Correspondence to:* B. Sreedhar (sreedharb@iict.res.in).

length of organoclays and ion exchange with protonated alkyl amines results in much larger interlayer distances in nanocomposites. Zilg et al.[6] reported that PU nanocomposites containing synthetic fluoromica could simultaneously increase their tensile strength and elongation at break. Ma et al.[8] intercalated an alkyl ammonium (hexadecyl-octadecyl trimethylammonium chloride) modified Na-montmorillonite into the polyol and prepared elastomeric PU (polypropylene glycol (PPG)/toluene diisocyanate (TDI)/glycerol propoxylate)/clay nanocomposite and found that at 8% clay loading, the tensile strength and the elongation at break of the PU/clay nanocomposite increased by two and five times than that of pure PU. Chen et al.[17] prepared a polycaprolactone (PCL)/clay nanocomposite from ε-caprolactone and 12-aminolauric acid modified-montmorillonite, which was subsequently added to PU (polycaprolactone diol/MDI/BD) in different ratio and studied the mechanical properties. They have shown that the crystallinity and the tensile mechanical properties of these PU/clay nanocomposites were strongly affected by the amount of PCL/clay. In another report, Chen et al.[7] studied the effect of organoclay concentration on the properties of PU/clay nanocomposite. They prepared PU/clay nanocomposite by using Na-montmorillonite treated with 12-aminolauric acid and benzidine. The twofold increase in tensile strength and threefold increase in elongation as compared with those of single PU were obtained by adding 1 wt % modified organoclay in PU composition. Another study from the same group[10] have observed a reduction in the degree of hydrogen bonding in the hard segments of PU because of the presence of the silicate layers, and the resultant morphology of the segmented polyurethane was altered. The extent of the reduction between the hydrogen bonding in the hard segment depends on the amount of the silicate layers and their dispersion. To improve the thermal durability[11] and tensile-mechanical properties[10] of polyurethane by silicates, Wei and coworkers modified montmorillonite with reactive swelling agents containing one to three hydroxyl groups. Yao et al.[9] have observed a decrease in thermal conductivity with an increase in the loading of layered clay to a polyether-urethane matrix. Solarski et al.[16] obtained an intercalated structure with improved thermal stability. An improvement in the flammability along with other physical properties was also observed using the unique interface that was developed with layered silicates with various resins.[18–24] Additionally, the incorporation of plate like nanoparticles with high aspect ratio results in the enhancement of the permeation-barrier properties of polymers[2,25] due to reduction in straightway movement of the water as well as oxygen molecule, which results in increasing the effective path length for diffusion. Since the permeability of the nanocomposites is markedly decreased, therefore, Giannelis[26] has attributed the increased thermal stability to the hindered out-diffusion of the volatile decomposition products. From the electrochemical measurements, Yang et al.[27] concluded that PU/clay films even in small amount of clay loading showed greater corrosion protection effect in 5 wt % aqueous NaCl electrolyte environment than the pure PU film. In general, the dispersion of clay nanolayers and the morphology of the nanocomposite depend on various factors, such as the mixing method (melt/solution intercalation), mixing time and temperature, solvent used, solvent concentration, size of the monomer or polymer, intercalation agent, and ion-exchange yield.[28,29]

We have synthesized and characterized different moisture cured PU-urea and PU-urea/clay nanocomposites for the application in coatings. Two series of PU-urea from PEG-1000 and PPG-1000 were prepared by reacting with 4,4′-diphenylmethane diisocyanate (MDI) in the presence and absence of trimethylol propane (TMP). The synthesized —NCO terminated PUs were reacted with atmospheric moisture and resulted in urea crosslinking. Ultrasonication was used for dispersing the modified K10 into the synthesized —NCO terminated PUs. The structural characterization in the present study includes Fourier transform infrared (FTIR), thermogravimetric analysis (TGA), differential scanning calorimetric (DSC), and XPS-spectrophotometer.

## EXPERIMENTAL

### Materials

PEG-1000, PPG-100, TMP, MDI, and untreated clay particle K10 were procured from Aldrich Chemicals (Milwaukee, WI), and cetyl trimethyl ammonium bromide (CTAB) and ethyl acetate from S.D. Fine Chem., Mumbai, India, were used. Solvents were stored over activated 3–4 Å molecular sieves.

### Method

A detailed synthetic method of PU-urea will be found elsewhere.[30,31] In brief, NCO-terminated polymers of MDI and PEG or PPG were prepared in the absence of any catalyst and with a NCO:OH equivalent weight ratio 1:1, 1.3:1 and 2:1. Similarly polymers with NCO:OH equivalent weight ratio of 1:1 and 1.3:1 and 2:1 were prepared in the presence of fixed amount of TMP. The reaction process follows by the removal of absorbed water by azeotropic mixture with toluene and then the water free PEG and TMP mixture was added to the kettle at 60–70°C and the reaction continued at 70–80°C for 12 h in $N_2$ environment. To remove the oligomeric part and the moisture reacted part, MDI was heated and filtered by a cloth before

use. The synthesized isocyanate-terminated polymers were reserved in plastic bottles. A part of the polymer was taken in Teflon disc and kept in an oven at 80°C for 6 h, and then the obtained polymer film was kept at room temperature and humidity for long time until the complete disappearance of NCO band in FTIR spectrum was observed. K10 was used for the preparation of nanocomposites. This type of clay belongs to the MMT family and is naturally hydrophilic and therefore hinders the dispersion of the clay particles in most polymer matrices. K10 belongs to the smectite family, characterized by negatively charged aluminosilicate layers bound by electrostatic forces by potassium ion located in the interlayer space. To increase the compatibility between the hydrophobic polymer and the hydrophilic clay, and to increase the interlayered spacing of the clay, swelling agent CTAB was used in this study. The organifier was dissolved in deionized water at 60°C and concentrated HCl was added drop by drop into the organifier solution to quaternize the amine group. Appropriate amount of K10 was preliminarily dispersed in deionized water at 60°C by using ultrasound probe attached to Malvern Mastersizer 2000 (UK) particle size analyzer (20 W $cm^{-2}$). The organifier solution was poured into the suspension containing K10 and the mixture was vigorously sonicated for 2 h. This technique is commonly employed when both high speed and high shear are required to create colloidal dispersion of the fine particles.[32] To avoid the excess heat generated during sonication, the sonication was repeatedly carried out in an alternate sonication and cooling cycle of around 30 s. After sonication, the cation-exchanged clay particles were collected by centrifuge and subsequently washed with deionized water. The treated K10 clay was washed repeatedly with deionized water. To ensure the complete removal of chloride ions, the filtrate was titrated with 0.1*N* $AgNO_3$ until no further AgCl precipitated. The product was then placed in a vacuum oven at 80°C for 12 h. The dried product was ground to get the organo-montmorillonite (*o*-K10). *o*-K10 (3 wt %) was used for nanocomposite preparation. For the preparation of nanocomposites, a 10 wt % transparent solution of the *o*-K10 in ethyl acetate was prepared, then added dropwise to a 10 wt % ethyl acetate solution of the synthesized polymers, and ultrasonicated for 2 h at 80°C.[25] The mixture was then poured onto teflon disc and kept in an oven at 80°C for 6 h and then the obtained polymer film was kept at room temperature and humidity for a long time until the complete disappearance of NCO band in FTIR spectrum was observed. Sample nomenclature, composition, and their NCO:OH ratio are shown in Table I. Polyurethane–urea (PU-urea) samples were denoted by PU and with different numbers ranging from 1 to 8 depending on the equivalent weight ratio of the monomers used, whereas the PU-urea/*o*-K10 nanocomposites were denoted by the word N at the end of PU-urea sample name. The PU-urea and the nanocomposite samples thus obtained were used for TGA, DSC, and XPS study.

**TABLE I**
**Details of the Sample Synthesized and the Abbreviations Used**

| Sample name | Composition (g) | NCO/OH equivalent weight ratio |
|---|---|---|
| PU-1 | PEG: 5.0 | 2:1 |
| PU-2 | PEG: 5.0; TMP: 0.5 | 1:1 |
| PU-3 | PEG: 5.0; TMP: 0.5 | 1.3:1 |
| PU-4 | PEG: 5.0; TMP: 0.5 | 2:1 |
| PU-5 | PPG: 5.0 | 2:1 |
| PU-6 | PPG: 5.0; TMP: 0.5 | 1:1 |
| PU-7 | PPG: 5.0; TMP: 0.5 | 1.3:1 |
| PU-8 | PPG: 5.0; TMP: 0.5 | 2:1 |

### FTIR instrumentation

For the FTIR study, a small and diluted drop of the liquid polymers as well as nanocomposites (typically a 1 wt % solution in ethyl acetate) were prepared and coated on KBr disks and stored at room temperature and humidity for a day before spectral evaluation. To remove the residual solvent, the disks were placed in a vacuum oven at 80°C for 6 h. The thickness of sample was controlled to have the same uniform size. Fourier transform IR spectra (FTIR) were obtained using a Thermo Nicolet Nexus 670 spectrometer. A minimum of 32 scans was signal-averaged with a resolution of 2 $cm^{-1}$ within the wavelength range of 400–4000 $cm^{-1}$.

### Thermal analysis

Thermogravimetric experiments were performed using a TGA/SDTA 851$^e$ thermal system (Mettler Toledo, Switzerland) at a heating rate of 10°C $min^{-1}$ in the temperature range of 25–800°C under $N_2$ atmosphere (flow rate, 30 mL $min^{-1}$). Film samples ranging from 8 to 10 mg were placed in the sample pan and heated. During the heating period, the weight loss and temperature difference were recorded as a function of temperature. Calorimetric measurements were carried out on a Mettler Toledo 821$^e$ DSC system (Zurich, Switzerland) in the temperature range of –60 to 200°C, at a heating rate of 10°C $min^{-1}$ under nitrogen atmosphere (flow rate, 30 mL $min^{-1}$). The instrument was calibrated with indium standards before measurements.

### XPS analysis

XPS is one of the most popular and useful technique for analyzing the surface compositions of coatings.

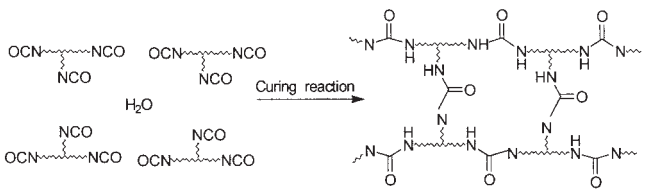


**Scheme 1** The curing reaction of NCO terminated prepolymer with moisture.

XPS probes a coating layer to a depth of about 7.5 nm. Angle resolved XPS is a technique by which a thin layer can be analyzed, with the sample tilted by changing the angle of the surface with respect to the detector. At high takeoff angles, the detector will only collect the emitted photoelectrons and auger electrons from the shallow region near the surface. At small takeoff angles, the detector will collect emitted electrons from both the shallow region and the deeper layers. Therefore, with a change in the takeoff angle, a concentration depth profile can be obtained. KRATOS AXIS 165 X-ray photoelectron spectrometer (UK) was used for the surface analysis. The X-ray gun was operated at 15 kV voltage and 20 mA. Survey and high-resolution spectra were collected using 80 and 40 eV pass energy, respectively. Before the experiment, the analyzer chamber was degasified and the pressure was kept as low as $\sim 1.33 \times 10^{-6}$ Pa. A thin film of thickness 0.1 mm was used for XPS-analysis. Survey scans were taken over a binding energy range of 0–1200 eV and then the narrow scan spectra of Si 2p, C 1s, O 1s and N 1s were collected. The XPS analysis was done at room temperature at two different electron take-off angles, namely 0 and 45°. The sample was tilted in such a way to change the angle $\theta$ between the normal to the sample and the analyzer. At $\theta = 0°$, the sample was perpendicular to the detector, leading to the maximum sampling depth. The effective sampling depth, $z$, was derived by $z = 3\lambda \cos \theta$, where $\lambda$ is the effective mean free path for electrons to escape the surface and was set to the value of 2.5 nm. Therefore at $\theta = 0°$, $z = 7.5$ nm and at $\theta = 45°$, $z = 5.3$ nm. Using the VISION software the observed peaks were deconvoluted in Gaussian/Lorentzian ratio 7:3. All spectra presented are charge balanced and the binding energy referenced to C 1s at 284.6 eV.

## RESULTS AND DISCUSSION

The formation of crosslinked PU-urea follows the general reaction of excess isocyanate in the prepolymer with moisture as shown in Scheme 1. The reaction demonstrates the basic structural backbone of the polyurethane polymer. However, structural crosslinks and microstructures within this system can provide additional structure within the polymer matrix by self-crosslinking and allophanate linkage formation from the reaction between the NCO and urethane groups.

### FTIR analysis

Of particular interest is the band due to NCO functionality at 2273 $cm^{-1}$, because its intensity is proportional to the concentration changes of the NCO groups. The byproduct formation, if any due to the reaction of moisture or other chemical moieties within the PU-urea matrix remain difficult to identify. The FTIR spectrum of *o*-K10 (organo modified) is shown in Figure 1(a). In Figure 1(b), PU-urea nanocomposites show a band at 2273 $cm^{-1}$ due to NCO group, and the intensity of the absorbance at 2273 $cm^{-1}$ decreased and disintegrates completely after the completion of NCO group reaction with atmospheric moisture. At the same time, the bands due to urea linkages, including N—H stretching and deformation bands at 3395

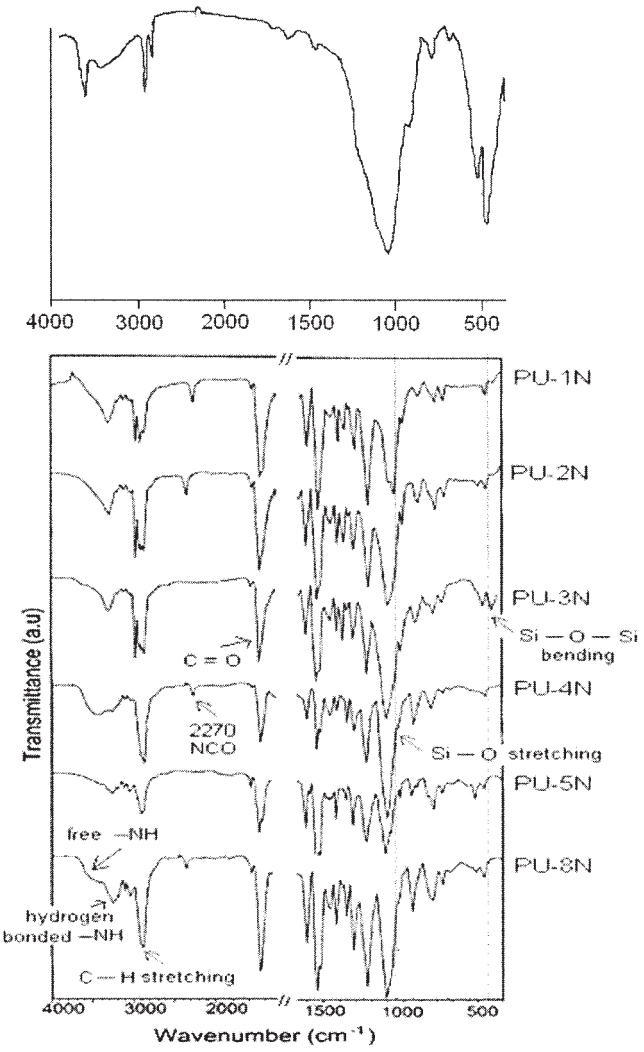


**Figure 1** FTIR spectra of modified K-10 (at the top) and different nanocomposite coatings (at the bottom).

**TABLE II**
**Thermal Stability Data of PU-urea/*o*-K10 Nanocomposite Coatings**

| Sample no. | $T_{ON}$ | $T_{MAX}$ | $T_{EN}$ | % wt 300°C | % wt 450°C | % wt 600°C |
|---|---|---|---|---|---|---|
| PU-1 | 316.5 | 424.2 | 440.3 | 94.7 | 28.2 | 20.6 |
| PU-1N | 318.1 | 425.4 | 443.3 | 97.7 | 30.5 | 24.5 |
| PU-2N | 318.6 | 426.6 | 441.7 | 99.0 | 31.9 | 25.1 |
| PU-3N | 303.4 | 426.6 | 535.6 | 97.6 | 37.9 | 26.3 |
| PU-4N | 302.9 | 427.9 | 541.7 | 96.4 | 44.3 | 27.6 |
| PU-5 | 305.1 | 363.0 | 396.2 | 95.7 | 25.9 | 17.0 |
| PU-5N | 321.4 | 380.9 | 409.9 | 97.4 | 31.3 | 23.3 |
| PU-6N | 323.0 | 389.1 | 410.9 | 99.0 | 31.4 | 25.3 |
| PU-7N | 315.8 | 422.0 | 438.4 | 97.4 | 37.0 | 27.8 |
| PU-8N | 324.3 | 422.8 | 440.8 | 99.4 | 40.5 | 34.3 |

and 1525 $cm^{-1}$, respectively, increase as crosslinking reaction progress. The FTIR spectra of PU-urea and PU/*o*-K10 are mainly characterized by bands at 3150–3600 $cm^{-1}$ (NH stretching vibrations), 2800–3000 $cm^{-1}$ (C—H asymmetric and symmetric stretching vibrations), 1600–1800 $cm^{-1}$ (C═O stretching vibrations), 1540 $cm^{-1}$ (amide II, $\delta_{N—H} + \nu_{C—N}$), 1240 $cm^{-1}$ (amide III, $\delta_{N—H} + \nu_{C—N}$), and at 1015, 1108, and 1227 $cm^{-1}$, which are due to C═O═C vibration arise from ether group in the soft segment.[27] The hydrogen-bonded NH peaks at 3290–3307 $cm^{-1}$, free NH peaks at 3527 $cm^{-1}$, and carbonyl peaks at 1701 and 1725 $cm^{-1}$ indicate the presence of urethane linkages.[33] Besides these bands, PU/*o*-K10 also has the characteristic bands of montmorillonite at 1038, 524, and 462 $cm^{-1}$, which correspond to the stretching vibration of Si—O—Si, the stretching vibration of Al—O and the Si—O bending vibration of montmorillonite respectively, which indicates the presence of layered silicate framework in the nanocomposite.[4,17,34]

### Dynamic thermogravimetric analysis

The thermal stability of PU-urea samples and their clay nanocomposites were investigated by thermogravimetric analyzer. The relative thermal stabilities of pure PU-urea and PU-urea/*o*-K10 hybrids are listed in Table II. The values of $T_{ON}$ (initial decomposition temperature for the first step of decomposition), $T_{MAX}$ (temperature of maximum rate of weight loss for the first step), $T_{EN}$ (final decomposition temperature), % weight loss at 300, 450, and 600°C, respectively, are shown in Table II. The nature of the DTG curves showed the complexity of the degradation following a number of steps of which two major steps are involved. In this study, we are mainly interested on the major decomposition step and the corresponding thermal data. On a comparison of the thermal stability data PU-urea/*o*-K10 nanocomposites derived from PEG-1000 and with increasing crosslinker content, one can see that the $T_{MAX}$, $T_{EN}$, and % wt remains at 450 and 600°C increases with increasing TMP and/or MDI content. For instant % wt at 450 and 600°C of PU-1N, PU-2N, PU-3N, and PU-4N were 30.5, 24.5; 31.9, 25.1; 37.9, 26.3; and 44.3, 27.6, respectively. Similarly for PPG based PU-urea/*o*-K10 nanocomposites coatings, $T_{MAX}$, $T_{EN}$, and % wt remains at 450 and 600°C increased with the increasing hard segment content. A comparison of the thermal stability data between PU-urea sample and the corresponding 3 wt % loaded nanocomposites shows that, thermal stability improves for both the PEG- and PPG-based coatings. For instance, the $T_{ON,}$ $T_{MAX,}$ $T_{EN,}$ and % wt remains at 300, 450, and 600°C of PU-1 and PU-1N were 316.5, 424.2, 440.3, 94.7, 28.2, 20.6 and 318.1, 425.4, 443.3, 97.7, 30.5, 24.5, respectively. Therefore, the general trend of the curves as shown in Figures 2(a) and 2(b) and the corresponding thermal data in Table II allows us to conclude that PU-urea/*o*-K10 have better thermal stability than PU-urea samples, and the thermal stability increased with increasing NCO/OH ratio.

This increase in the thermal stability could be attributed to the high thermal stability of the clay and the interaction between the clay particles and the PU-urea matrix.[35] Since the chain motions of polymer molecules in these silicate layers were barred and limited, therefore, thermal properties of PU-urea/*o*-K10 nanocomposites increased.[12] The other probable cause will be the layered silicates of *o*-K10, make the path longer for escaping of the thermally decomposed volatiles, or in other words clay particles can enhance the thermal stability of the polymer by acting as thermal insulator and mass transport barrier to the volatile products generated during decomposition. Similar trends have been noted in other articles also.[4,29,36–39]

### DSC analysis

An endotherm is observed in the DSC thermograms in between 40 and 120°C, which could be due to the short range ordering interaction within the PU-urea or the nanocomposites samples. The glass transition temper-

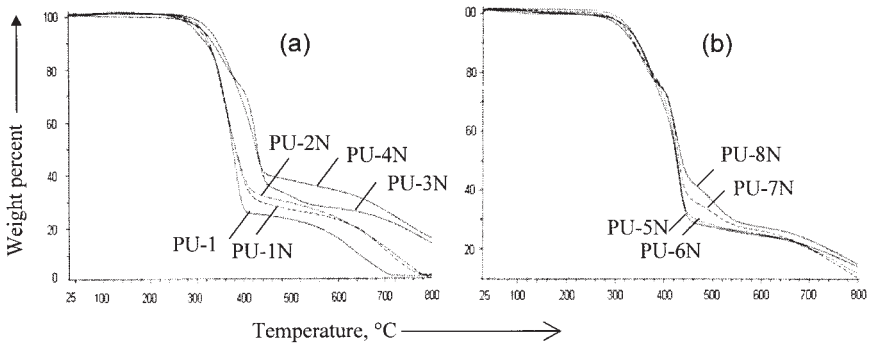


**Figure 2** Dynamic TG thermograms of PU-urea and PU-urea/*o*-K10 nanocomposite coatings in nitrogen environment.

ature of the soft segment for the PU-urea samples increased with the increasing hard segment content in the sample. For instance, the $T_g$ values of PU-1, PU-2, and PU-3 were −29.8, −13.5, and −9.0°C, respectively, whereas the soft segment $T_g$ completely disappears for PU-4, which could be due to the phase mixing process between the soft and hard segments associated during the moisture cure (Table III). The glass transition temperatures of the PU-urea/clay nanocomposites containing different amounts of the crosslinker were measured by using DSC at a scanning rate of 10°C $min^{-1}$ and are shown in Figure 3. With the addition of clay, the $T_g$ peak moved toward higher temperature and a decrease in peak intensity was observed. For example, the $T_g$ values of PU-1 and PU-1N were −29.8 and −28.0°C, respectively. This phenomenon was attributed to the confinement of the segmental motions of intermolecular chains of the PU-urea within the clay galleries or in other words to the restricted chain mobility at the interfacial layer, in which polymer chains are effectively anchored or attached to the silicate surface. These anchored polymer chains form an interphase region, where the segment relaxation is slower than in the bulk. The restricted relaxation behavior for the polymer nanocomposites with intercalated and exfoliated silicates depended primarily on the exfoliation extent of the layered silicates and the interaction strength between the silicate surfaces and the PU macromolecules. Thus, a system with fully exfoliated silicate dispersion and strong interactions is expected to exhibit slow relaxation behavior, while a system with intercalated silicates and relatively weak interaction should display fast relaxation dynamics. In addition, the overall relaxation behavior of the nanocomposites depends still on the ratio of restricted and unrestricted macromolecular segment numbers, related with the clay contents and its dispersion morphology.[40–43]

**TABLE III**
**Glass Transition Temperatures of PU-urea/o-K10 Nanocomposite Coatings**

| Sample name | $T_g$ (°C) |
|---|---|
| PU-1 | −29.8 |
| PU-1N | −28.0 |
| PU-2 | −13.5 |
| PU-2N | −10.0 |
| PU-3N | −9.5 |
| PU-5 | −7.8 |
| PU-5N | −0.8 |
| PU-6N | 0.1 |
| PU-7N | 5.3 |

## XPS analysis

In this technique, electrons emitted from atoms reside near the surface of the material escape without losing energy, and hence results in surface sensitive features. Therefore, a subtle change in peak positions and shape can yield quantitative information on changes in surface chemistry as well as a chemical depth profile information can be obtained by variation of the angle of incident of radiation. Simultaneously, the low resolution XPS has the ability to determine the elemental composition on the surface of all nonvolatile materi-

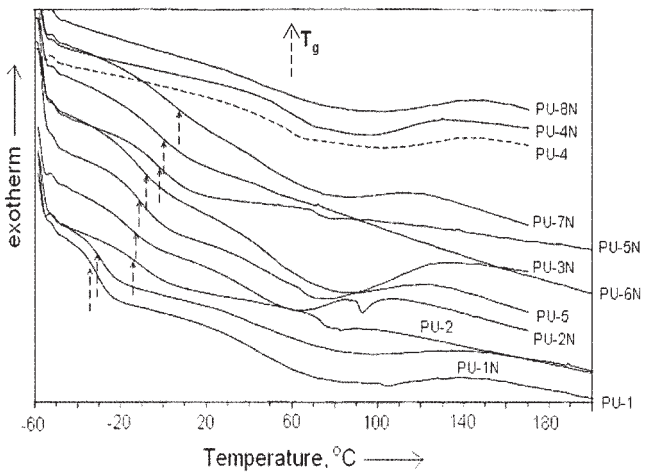


**Figure 3** DSC thermograms of PU-urea and PU-urea/*o*-K10 nanocomposite coatings in nitrogen environment.

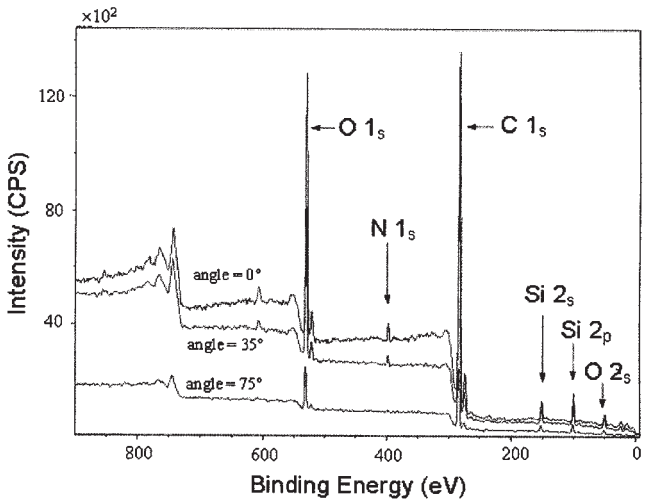


**Figure 4** Low resolution XPS survey scans of PU-1N nanocomposite at different takeoff angles.

als. Analysis of the XPS data gives an idea about the local oxidation states and chemical states of the composing material. In this study, the surfaces of nanocomposites polyurethane films were scanned and high resolution C 1s XPS spectra were recorded for extracting information about the studied samples. The peaks at binding energies of 96–116, 280–305, 396–416, and 528–548 eV are ascribed to the elements Si 2p, C 1s, N 1s, and O 1s, respectively. The survey spectra of PU-1N at different takeoff angle are shown in Figure 4. The characteristic features that are observed in the survey spectra is the decrease in N 1s peak intensity with increasing takeoff angle and a complete disappearance at 75°. This shows that the low surface energy polyether component resides toward the top surface and a high surface energy urethane/urea component resides inside the bulk of the polymer. Figure 5 shows the high resolution C 1s deconvoluted spectra at 0 and 45° takeoff angles of different PU-urea/*o*-K10 nanocomposites investigated.

The peak area of the carbons associated with different environments and peak area ratio of C—O at 45 and 0° from the deconvoluted spectra are shown in Table IV. In this study, the variation in the content of hard segment was attained by changing the weight ratio of polyether glycol, TMP, and MDI. Clearly, an increase in the mole fraction of TMP and MDI in the system results to an increase in the hard segment content. The different recipes lead to different molecular geometrical structures, hard domains, and aggregates. Polyurethane coatings are well known about their surface segregation characteristics.[31] On application to a metal, say for example on iron, the urethane/urea segment segregation toward the metal has resulted an improved adhesion characteristics, whereas the segregation of low surface energy component, e.g., the soft ether group toward the air interface results in dart repellant characteristics. Therefore, the distribution of C—O (originated from the polyether segment), C—N, and C═O (arises from the urethane/urea groups) groups have a depth dependence character in the PU-urea/*o*-K10 nanocomposite films. In this circumstance, we assume that the C—C/C—H distribution is constant throughout the film. Now a comparison of C—O/(C—C/C—H) peak area ratio at 45 and 0° of the investigated coatings suggests that the ratio decreased with decreasing takeoff angle. For instance, for PU-1N coatings the C—O/(C—C/C—H) ratio at 45 and 0° are 1.704 and 0.801. A similar trend was also observed for other nanocomposite coatings. These results suggest that the soft segment preferentially re-

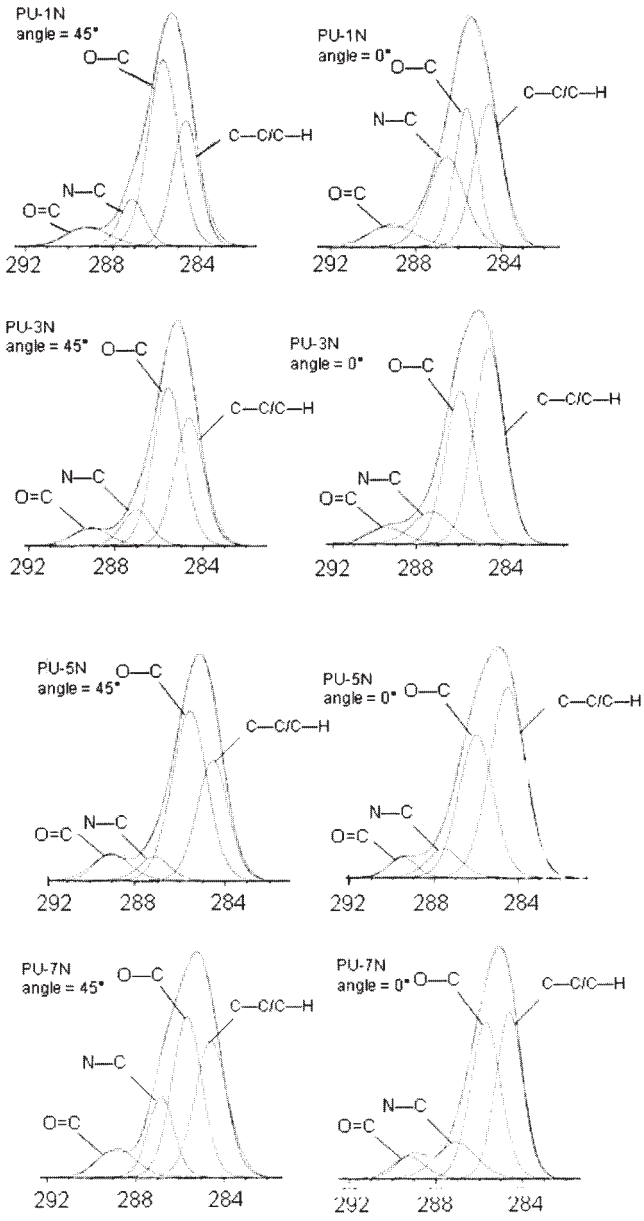


**Figure 5** The deconvoluted C 1s AR-XPS spectra of PU-urea/*o*-K10 nanocomposites at takeoff angle 45° and 0°.

**TABLE IV**
**The Deconvoluted C 1s Peak Area Associated with Carbons in Different Environment and their Ratio**

| Sample | C—C/C—H (284.5−284.7 eV) area% | C—O (285.6−286.0 eV) area% | C—N (286.6−287.5 eV) area% | C═O (288.8−289.5 eV) area % | C—O/(C—C/C—H) (area ratio) | C—O (45°)/C—O) (0°) (area ratio) |
|---|---|---|---|---|---|---|
| PU-1N (45°) | 30.4 | 51.8 | 10.5 | 7.2 | 1.704 | 1.836 |
| PU-1N (0°) | 35.2 | 28.2 | 28.0 | 8.6 | 0.801 | |
| PU-3N (45°) | 36.7 | 47.3 | 9.8 | 6.2 | 1.288 | 1.281 |
| PU-3N (0°) | 48.4 | 36.9 | 9.9 | 4.8 | 0.762 | |
| PU-5N (45°) | 33.0 | 52.0 | 6.2 | 8.8 | 1.575 | 1.397 |
| PU-5N (0°) | 51.8 | 37.2 | 7.1 | 4.0 | 0.718 | |
| PU-7N (45°) | 35.0 | 39.5 | 16.8 | 8.8 | 1.128 | 0.949 |
| PU-7N (0°) | 39.3 | 41.6 | 13.0 | 6.2 | 1.058 | |

sides on the top surface of the polymer. A comparison of C—O (45°)/C—O (0°) peak area ratio of the studied nanocomposite PU-1N and PU-3N coatings suggests a reduction of this ratio from 1.836 to 1.28. Similarly for PPG-based nanocomposite coatings PU-5N and PU-7N, this ratio reduces from 1.397 to 0.949. This phenomenon was due to the phase mixing process with increasing TMP and/or MDI content in the coatings. Since the phase mixing hinders the segregation nature of the soft polyether chain and hard segment, the contribution of C—O to the total C 1s peak area at the top surface, i.e., at 45° reduces and an enhancement in the bulk, i.e., at 0°, takes place. This phenomenon results in a decrease in C—O (45°)/C—O (0°) ratio in PU-3N and PU-7N in comparison with PU-1N and PU-5N.

## CONCLUSIONS

The properties of the nanocomposites based on organically-modified clay particles depend on the technique used to achieve the dispersion and on the cure temperature of the system. The data presented in this paper were obtained using ultrasonication to assist the dispersion process. In most cases, the interaction of the 3 wt % loaded clay with the resin leads to a reinforcing action with observation of an increase in the thermal stability and glass transition temperatures. The glass transition temperature of the PU-urea increased slightly with the addition of clay. The thermal stability of the PU-urea increased moderately after the incorporation of clay. An increase in NCO:OH ratio and introduction of TMP have resulted with improved thermal properties of the nanocomposite coatings because of the phase mixing process. High resolution XPS analysis was used to provide a method of differentiating the presence of different types of carbon bonds in the studied nanocomposites. The surface segregation phenomenon and the phase mixing process with increasing NCO:OH ratio was confirmed from the high resolution C 1s deconvoluted spectra.

D. K. Chattopadhyay acknowledges the receipt of a University Grants Commission (UGC, India) award for research fellowship in Engineering and Technology.

## References

1. Varma, A. J.; Deshpande, M. D.; Nadkarni, V. M. Angew Makromol Chem 1985, 132, 203.
2. Osman, M. A.; Mittal, V.; Morbidelli, M.; Suter, U. W. Macromolecules 2003, 36, 9851.
3. Gleiter, H. Prog Mater Sci 1989, 33, 223.
4. Takeichi, T.; Guo, Y. J Appl Polym Sci 2003, 90, 4075.
5. Wang, Z.; Pinnavaia, T. J Chem Mater 1998, 10, 3769.
6. Zilg, C.; Thomann, R.; Mulhaupt, R.; Finter, J. Adv Mater 1999, 11, 49.
7. Chen, T. K.; Tien, Y. I.; Wie, K. H. Polymer 2000, 41, 1345.
8. Ma, J.; Zhang, S.; Qi, Z. J Appl Polym Sci 2001, 82, 1444.
9. Yao, K. J.; Song, M.; Hourston, D. J.; Luo, D. Z. Polymer 2002, 43, 1017.
10. Tien, Y. I.; Wei, K. H. Polymer 2001, 42, 3213.
11. Tien, Y. I.; Wei, K. H. Macromolecules 2001, 34, 9045.
12. Ni, P.; Li, J.; Suo, J.; Li, S. J Appl Polym Sci 2004, 94, 534.
13. Mishra, J. K.; Kim, I.; Ha, C.-S. Macromol Rapid Commun 2003, 24, 671.
14. Han, B.; Cheng, A.; Ji, G.; Wu, S.; Shen, J. J Appl Polym Sci 2004, 91, 2536.
15. Pinnavaia, T. J. Science 1983, 220, 365.
16. Solarski, S.; Benali, S.; Rochery, M.; Devaux, E.; Alexandre, M.; Monteverde, F.; Dubois, P. J Appl Polym Sci 2005, 95, 238.
17. Chen, T. K.; Tien, Y. I.; Wei, K. H. J Polym Sci Part A: Polym Chem 1999, 37, 2225.
18. Gilman, J. W. Appl Clay Sci 1999, 15, 31.
19. Zhu, J.; Morgan, A. B.; Lamelas, J.; Wilkie, C. A. Chem Mater 2001, 13, 3774.
20. Zanetti, M.; Camino, G.; Mulhaupt, R. Polym Degrad Stab 2001, 74, 413.
21. Kojima, Y.; Usuki, A.; Kawasumi, M.; Okada, A.; Fukushima, Y.; Karauchi, T.; Kamigaito, O. J Mater Res 1993, 8, 1185.
22. Kawasumi, M.; Hasegawa, N.; Kato, M.; Usuki, A.; Okada, A. Macromolecules 1997, 30, 6333.
23. Wang, Z.; Pinnavaia, T. J. Chem Mater 1998, 10, 1820.
24. Manias, E.; Touny, A.; Wu, L.; Strawhecker, K.; Lu, B.; Chung, T. C. Chem Mater 2001, 13, 3516.
25. Xu, R.; Manias, E.; Snyder, A. J.; Runt, J. Macromolecules 2001, 34, 337.
26. Giannelis, E. P. Adv Mater 1996, 8, 29.
27. Yang, Y. W. C.; Yang, H. C.; Li, G. L.; Li, Y. K. J Polym Res 2004, 11, 275.
28. Takeichi, T.; Zeidam, R.; Agag, T. Polymer 2002, 43, 45.

29. Chang, J. H.; An, Y. U. J Polym Sci Part B: Polym Phys 2002, 40, 670.
30. Chattopadhyay, D. K.; Sreedhar, B.; Raju, K. V. S. N. J Appl Polym Sci 2005, 95, 1509.
31. Chattopadhyay, D. K.; Sreedhar, B; Raju, K. V. S. N. Ind Eng Chem Res 2005, 44, 1772.
32. Rhoney, I.; Brown, S.; Hudson, N. E.; Pethrick, R. A. J Appl Polym Sci 2004, 91, 1335.
33. Pattanayak, A.; Jana, S. C. Polymer 2005, 46, 3275.
34. Zhang, X.; Xu, R.; Wu, Z.; Zhou, C. Polym Int 2003, 52, 790.
35. Kim, D. S.; Kim, J.-T.; Woo, W. B. J Appl Polym Sci 2005, 96, 1641.
36. Choi, W. J.; Kim, S. H.; Kim, Y. J.; Kim, S. C. Polymer 2004, 45, 6045.
37. Fischer, H. R.; Gielgens, L. H.; Koster, T. P. M. Acta Polym 1999, 50, 122.
38. Petrovic, X. S.; Javni, L.; Waddong, A.; Banhegyi, G. J. J Appl Polym Sci 2000, 76, 133.
39. Zhu, Z. K.; Yang, Y.; Yin, J.; Wang, X.; Ke, Y.; Qi, Z. J Appl Polym Sci 1999, 3, 2063.
40. Lu, H. B.; Nutt, S. Macromolecules 2003, 36, 4010.
41. Dai, X.; Xu, J.; Guo, X.; Lu, Y.; Shen, D.; Zhao, N.; Luo, X.; Zhang, X. Macromolecules 2004, 37, 5615.
42. Chen, Y.; Zhou, S.; Yang, H.; Gu, G.; Wu, L. J Colloid Interface Sci 2004, 279, 370.
43. Ma, X.; Lu, H.; Liang, G.; Yan, H. J Appl Polym Sci 2004, 93, 608.